Supporting Information

Highly-crystallized Fe_2P-embedded in N-doped carbon for enhancing long-term bio-electricity generation by lowering cathode poisoning in microbial fuel cells

Peng Zhang[a], Zhuang Cai[a], Shijie You[b], Fangyu Wang[a], Ying Dai[a,c,*], Yuan Lv[a], Yanhong Zhang[a,*], Nanqi Ren[b], Jinlong Zou[a,*]

[a] Key Laboratory of Functional Inorganic Material Chemistry, Ministry of Education of the People's Republic of China, School of Chemistry and Materials Science, Heilongjiang University, Xuefu Road 74#, Nangang District, Harbin, 150080, China;

[b] State Key Laboratory of Urban Water Resource and Environment, School of Environment, Huanghe Road 73#, Nangang District, Harbin Institute of Technology, Harbin 150090, P. R. China;

[c]School of Civil Engineering, Heilongjiang Institute of Technology, Hongqi Street 999#, Daowai District, Harbin 150050, China.

Corresponding author (s):

*Ying Dai, Yanhong Zhang, Jinlong Zou.

[a]Xuefu Road 74#, Nangang District, Harbin, 150080, China.

E-mail address:

zjh_0308@126.com (Y. Dai);

zhangyanhong@hlju.edu.cn (Y. H. Zhang);

zoujinlong@aliyun.com (J. L. Zou).

Number of pages: 21

Number of figures: 8

Number of tables: 4

Material characterization

X-ray diffraction (XPD) data were collected to pass a Rigaku D /max-Ⅲ diffractometer (λ = 1.5406 Å) at a step scan speed of 0.02° over the range of 10°-80°. The catalyst crystal structure data was analyzed according to the Joint Committee Powder Diffraction Standard (JCPDS). The nitrogen adsorption/desorption isotherms were measured at 77 K using the Micromeritics Tristar Ⅱ. The specific surface areas (S_{BET}) of composites were calculated by using Brunauere-Emmette-Teller (BET) method, meanwhile the pore size distributions were obtained by using Barrett-Joyner-Halenda (BJH) method. Scanning electron microscopy (SEM) images were taken on an S-4800 scanning electron microscope (Japan) at 5.0 kV. The images were used to investigate the internal structure of Fe_2P/NPGC-x. Transmission electron microscopy (TEM) images were obtained on the JEM-2100 electron microscope (JEOL) at 200 kV. X-ray photoelectron spectroscopy (XPS) tests were conducted on Kratos-AXISUL TRA DLD (Al Kα X-ray source) and the XPS data for each atom were fitted using the 'XPS peak' software.

Material electrochemical analysis

The ORR performances characterized by cyclic voltammetry (CV), linear sweep voltammetry (LSV), rotating disk electrode (RDE) and electrochemical impedance spectroscopy (EIS) were carried out on a CHI 760E electrochemical workstation (Shanghai Chenhua) in a three-electrode cell connected to a computer. The CV scan was performed in the potential range from −0.8 to +0.3 V at a scan rate of 50 mV s^{-1} in three-electrode system. The working electrode for CV was a glassy carbon electrode, which was 0.4 cm in diameter. The catalyst ink for CV test was prepared by adding 5mg well-dispersed samples into the mixed solution with 100 μm ethanol and 50 μm Nafion

(5 wt.% solution), then treated ultrasonically for 30 min. 5 μm ink suspension was dropped onto the glassy carbon electrode and dried in air. LSV tests were carried out by using the cathodes of MFCs as the working electrode, equipping with 1 cm^2 platinum sheet square counter electrode and an SCE reference electrode. It was measured at a scan rate of 1 mV s^{-1} on the cathodes of the tested MFCs with 28 mL of 50 mM PBS. The electrochemical impedance spectroscopy (EIS) was conducted at the open circuit voltage (V_{oc}) of 10 mV over a wide frequency range from 10^5 to 10^{-2} Hz. ZsimpWin 3.10 software (Echem, Lufkin, TX) to calculate charge transfer resistance (R_{CT}) by using the EIS data. The polarization and power density curves were acquired by varying the external resistance from 5000 to 50 Ω. The potassium dichromate oxidation method was used to test the chemical oxygen demand (COD) of effluents. The coulombic efficiency (CE) was calculated according to the previously reported method.[1]

The rotating disk electrode (RDE) test by changing different rotation rates (from 225 to 2025 rpm, and scan rate of 5 mV s^{-1}), what in O_2-saturated 50 mM PBS electrolyte. RDE test were obtained in the potential range from +0.6 to 1.0 V (vs Ag/AgCl), that the results according to the Koutecky-Levich (K-L) plots. Based on the K-L equation to calculate the average number of transferred electorns (n) from the following Eqs. 1:

$$\frac{1}{J} = \frac{1}{J_K} + \frac{1}{0.2nFC_O D_0^{2/3} v^{-1/6} \omega^{1/2}} \qquad (1)$$

where j, and j_K are the measured current density (mA cm^{-2}), and kinetic current density, respectively; F is the Faraday constant (96485 C mol^{-1}); C_O is the concentration of O_2 in PBS (1.2×10^{-6} mol cm^{-3}); D_O is the diffusion coefficient of O_2 in PBS (1.9×10^{-5} cm^2 s^{-1}); v is the kinematic viscosity of PBS (1.0×10^{-2} cm^2 s^{-1}); and ω is the rotation rate of the electrode.[2]

Electrode preparation for MFCs

Carbon fiber brush as the anode was washed by acetone and distilled water several times, which was then heated in air at 450 °C according to the previously reported method.[3] The gas diffusion layer (GDL) of the air cathode was prepared using the rolling method. Carbon black and 60 wt.% PTFE (mass ratio of 7: 3) were rolled onto stainless steel nets (60 mesh), which was then calcined at 340 °C for 30 min in a muffle furnace to obtain the GDL.[4] The catalyst mixed with PTFE (mass ratio of 2: 1) was uniformly rolled onto the other side of GDL, which was then dried at 80 °C in an oven. The Fe_2P/NPGC-x (750, 800, 850, 900 and 950) were used as the cathodic catalysts by comparing with the commercial Pt/C (10 wt.%, Hesen Electric Co., Ltd, Shanghai, China) catalyst. Escherichia coli (E. coli) bacteria are used as the electrogenic bacteria and inoculants to activate the reactors in our study, which have been already recognized as the efficient bacteria for MFCs.[1,3,5]

MFCs configuration and operation

The single-chamber reactor (air cathode) was consisted of a cylindrical plexiglas chamber, which had lengths of 4 cm, diameters of 3 cm and inner volume of approximately 28 mL.[6] The titanium wire was used to connect the two electrodes with external resistance of 1000Ω. Two rubber gaskets were used to prevent the air into the reactor. The electrolyte composed of phosphate buffered solution (PBS, pH=7.4), vitamins minerals (5 mL L^{-1}) and trace (12.5 mL L^{-1}) was the same as that of the previous study.[4] All of the reactors were operated at 30 °C. To achieve statistical soundness, each reactor at least had another two parallel samples.

Electrocatalytic activity of Fe_2P/NPGC in neutral solution

To evaluate the ORR catalytic activity, CV tests are performed for Fe_2P/NPGC-x (750, 800, 850, 900 and 950) and Pt/C catalysts in MFCs. As shown in Figure S7a, no redox peaks can be detected on CV curve, which may be caused by the limitation of the testing method.[6] The highest current density is still obtained by Fe_2P/NPGC-850 (–6.23 mA cm^{-2}), which is higher than those of Pt/C (–5.19 mA cm^{-2}) and other Fe_2P/NPGC composites. LSV tests are also conducted to evaluate the ORR activities of Fe_2P/NPGC and Pt/C. As shown in Figure S7b, Fe_2P/NPGC-850 has the maximum current density (−2.5 mA cm^{-2}), which is higher than that of Pt/C (−2.22 mA cm^{-2}), demonstrating that this catalyst may exhibit a favorably efficient ORR activity in MFCs, consistent with the results of CV tests. The high ORR catalytic activity is mainly attributed to the rapid capture and the low resistance transfer of oxygen.[5] Through XPS and FT-IR tests, oxygen-containing functional groups on the catalyst surface are confirmed to be present and enhancing the ability to capture oxygen in the electrolyte solution.[7-9] The S_{BET} tests show that the pore size of the Fe_2P/NPGC-850 catalyst is significantly larger than the diameter of the oxygen molecule, which enable the transportation of oxygen into the Fe_2P/NPGC-850 with hardly any resistance.[10] And, the N-doped structure improve the electronic activity of the outermost layer of adjacent C atoms, that provide the smooth transmission path for O_2.[11] Moreover, oxygen is quickly adsorbed to the Fe_2P surface by weakly basic P atoms, and the rapid cleavage of O−O bonds by Fe^{2+}, thus leading to an increase in the ORR efficiency.[12]

Table S1. Nitrogen atomic weight percentage (wt.%) of various chemical states in Fe_2P/NPGC-x (x=700 (a), 750 (b), 800 (c), 850 (d) and 900 (e)).

Samples	Pyridinic N	Pyrrolic N	Graphitic N	Total N
Fe_2P/NPGC-700	21.29	69.77	8.94	2.13
Fe_2P/NPGC-750	43.61	47.42	8.97	3.98
Fe_2P/NPGC-800	45.33	46.6	8.07	4.96
Fe_2P/NPGC-850	51.3	35.21	13.49	6.53
Fe_2P/NPGC-900	56.76	34.23	9.01	5.71

Table S2. Textural property of the Fe_2P/NPGC-x (x=700, 750, 800, 850 and 900) composites.

Samples	BET surface area (m^2 g^{-1})	Pore volume (cm^3 g^{-1})	Average pore width (nm)
Fe_2P/NPGC-700	16.86	0.03	6.20
Fe_2P/NPGC-750	20.18	0.06	7.41
Fe_2P/NPGC-800	24.63	0.06	7.60
Fe_2P/NPGC-850	33.77	0.07	10.02
Fe_2P/NPGC-900	26.85	0.06	8.73

1 **Table S3.** Summary of performances of various cathode catalysts in MFCs.

Catalysts	P_{MAX} (W m^{-2})	Voltage output (V)	Operation time (h)	References
Fe_2P/NPGC-850	1.05	0.535	1440	This work
Co_2P/NC-850	0.773	0.145	450	6
Fe/Fe_3O_4/FeS/NGC-900	0.93	0.59	2160	13
GO-Zn/Co-800	0.972	0.554	2000	14
CA-10KOH	0.967	0.39	500	15
C(N)/MnO_x-SP	0.467	0.35	450	16
MOF-800	0.326	0.365	720	17
GF-$CoMn_2O_4$/rGO	0.361	0.822	1680	18
Co-Al_2O_3-rGO	0.548	0.631	720	19
FePc/PID/CNTs	0.799	0.51	700	20

2

3

Table S4. The electrochemical impedance fitting results of Fe_2P/NPGC-x (x=700, 750, 800, 850 and 900).

Cathodes	R_0 (Ω)	R_{ct} (Ω)
Fe_2P/NPGC-700	3.334±0.4	24.1±0.3
Fe_2P/NPGC-750	3.178±0.2	21.3±0.5
Fe_2P/NPGC-800	2.954±0.3	18.5±0.3
Fe_2P/NPGC-850	1.679±0.2	9.5±0.4
Fe_2P/NPGC-900	2.674±0.3	16.6±0.4
Pt/C	2.172±0.2	11.6±0.5

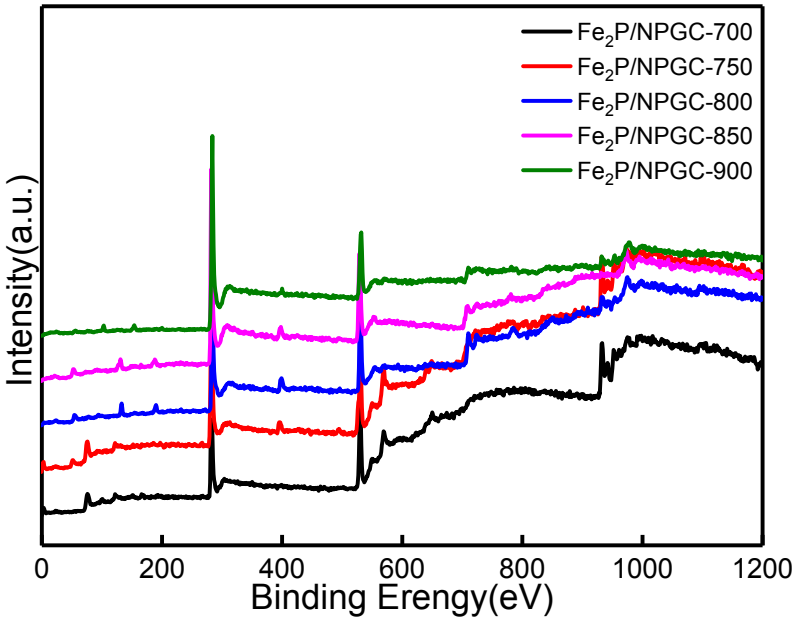

Figure S1. The XPS survey spectra of the Fe_2P/NPGC-x (x= 700, 750, 800 and 900).

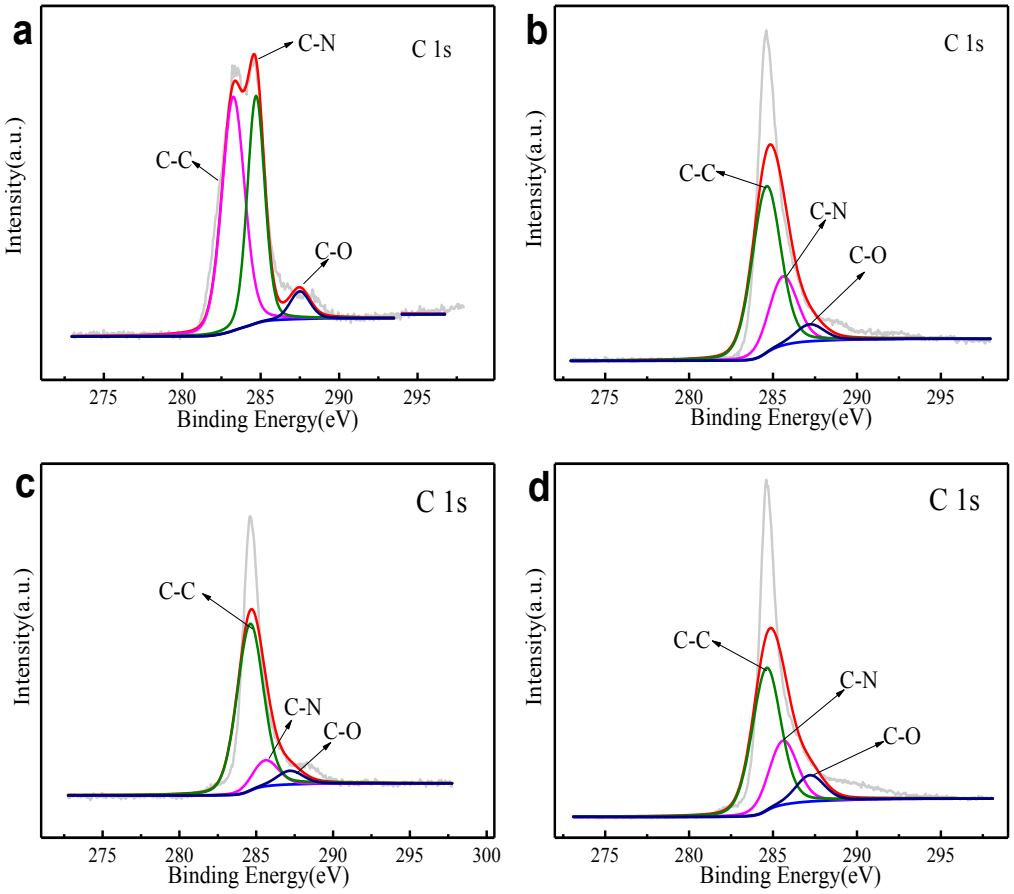

Figure S2. High resolution XPS spectra of C 1s of Fe_2P/NPGC-x (x= 700, 750, 800 and 900).

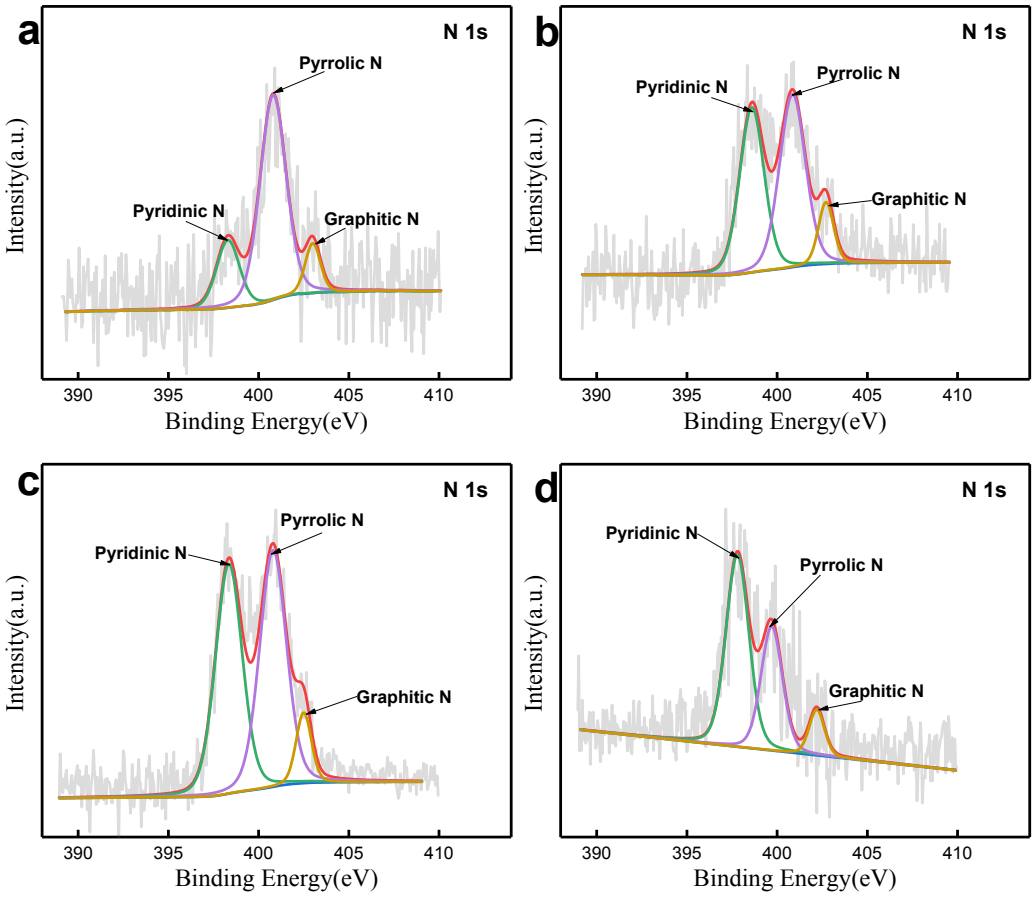

Figure S3. High resolution XPS spectra of N 1s of Fe_2P/NPGC-x (x= 700, 750, 800 and 900).

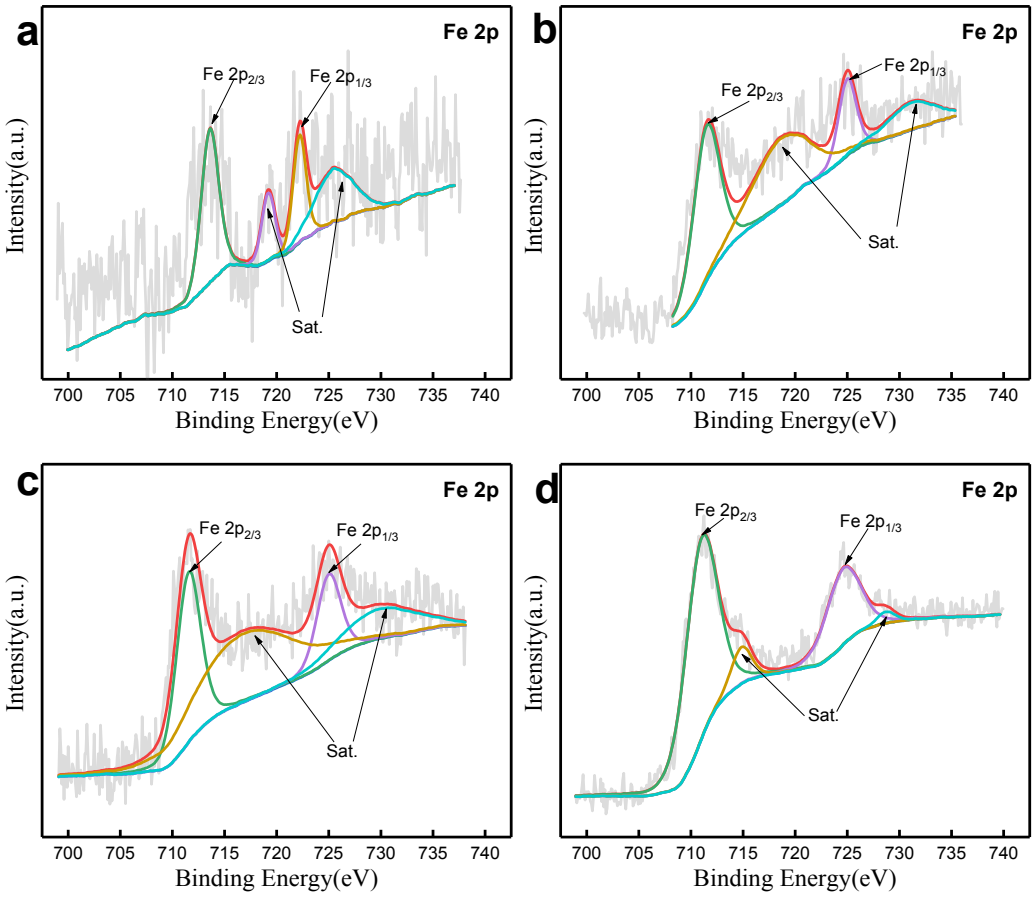

Figure S4. High resolution XPS spectra of Fe 2p of Fe_2P/NPGC-x (x= 700, 750, 800 and 900).

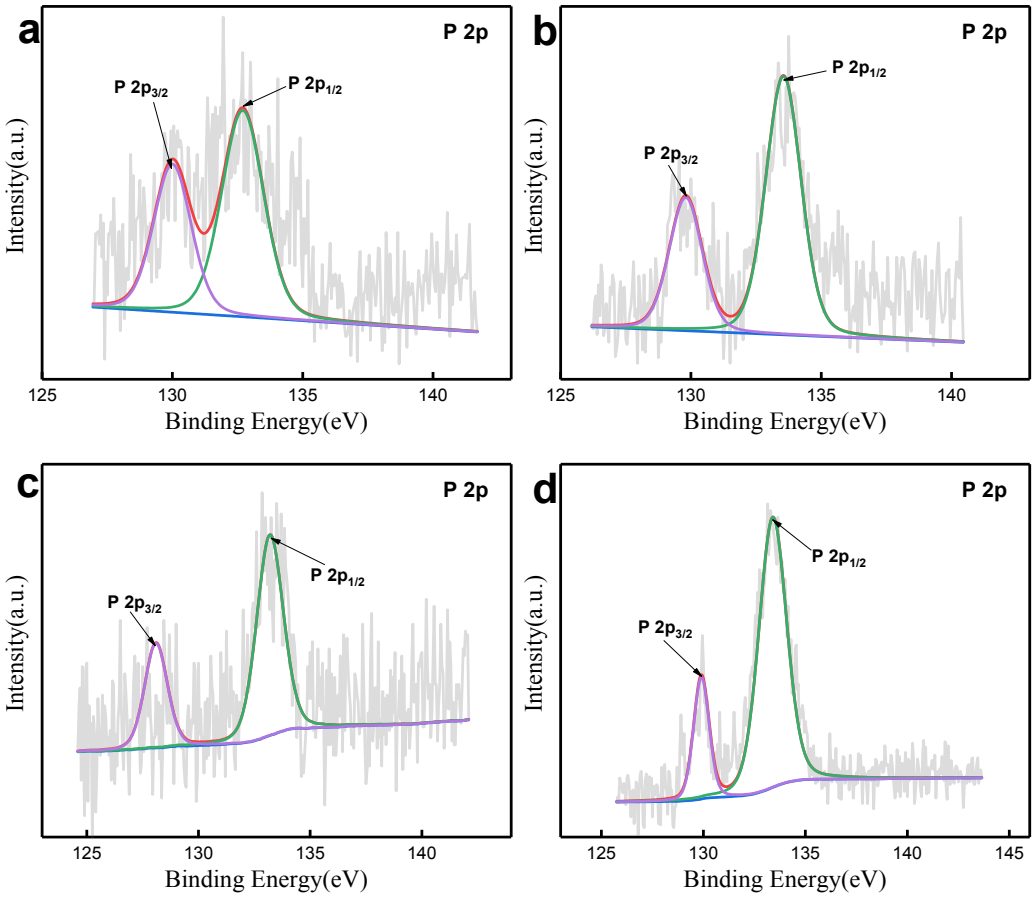

Figure S5. High resolution XPS spectra of P 2p of Fe_2P/NPGC-x (x= 700, 750, 800 and 900).

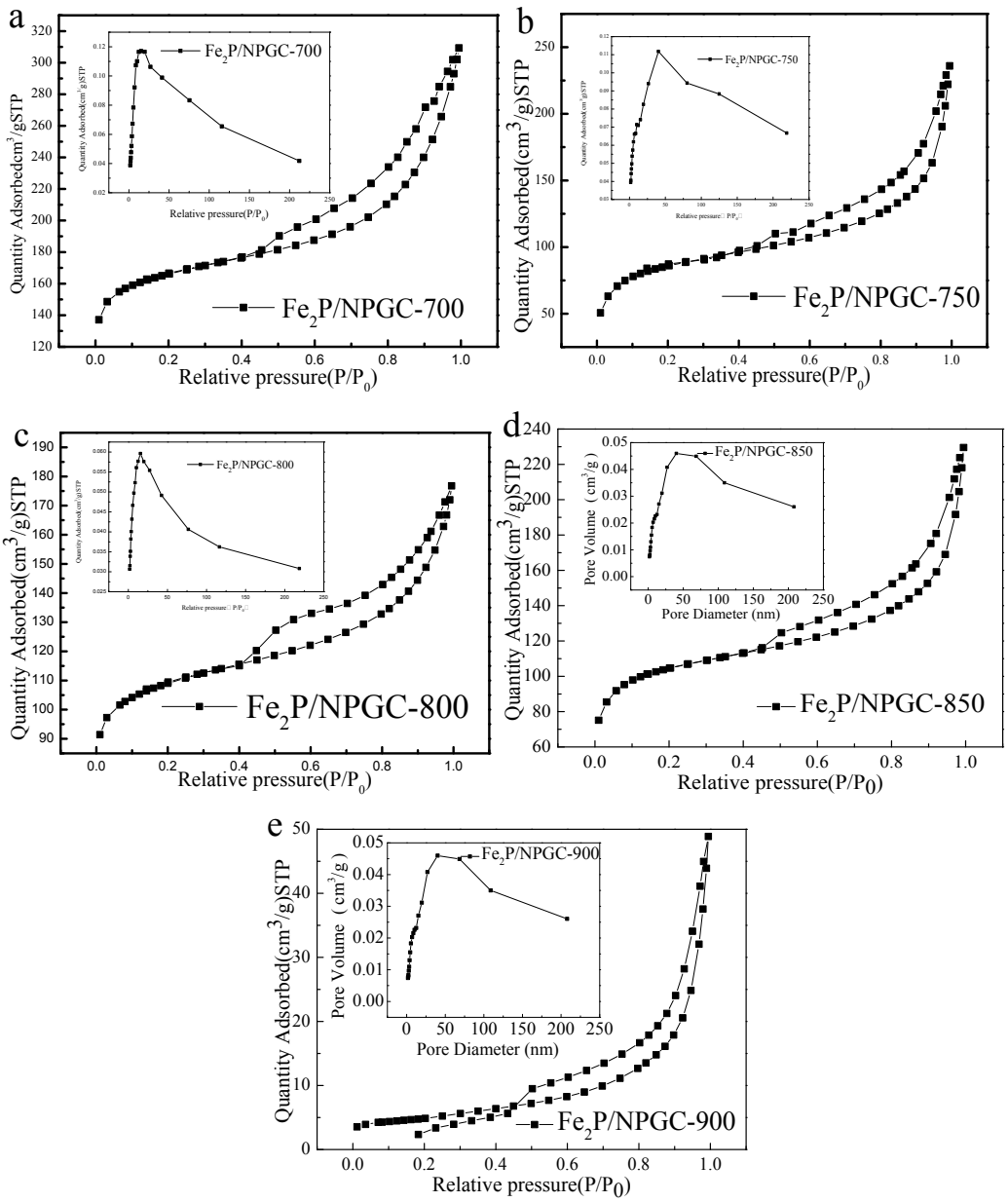

Figure S6. N_2 adsorption/desorption isotherms and pore size distributions (inset) for the Fe_2P/NPGC-x (x=700, 750, 800, 850 and 900).

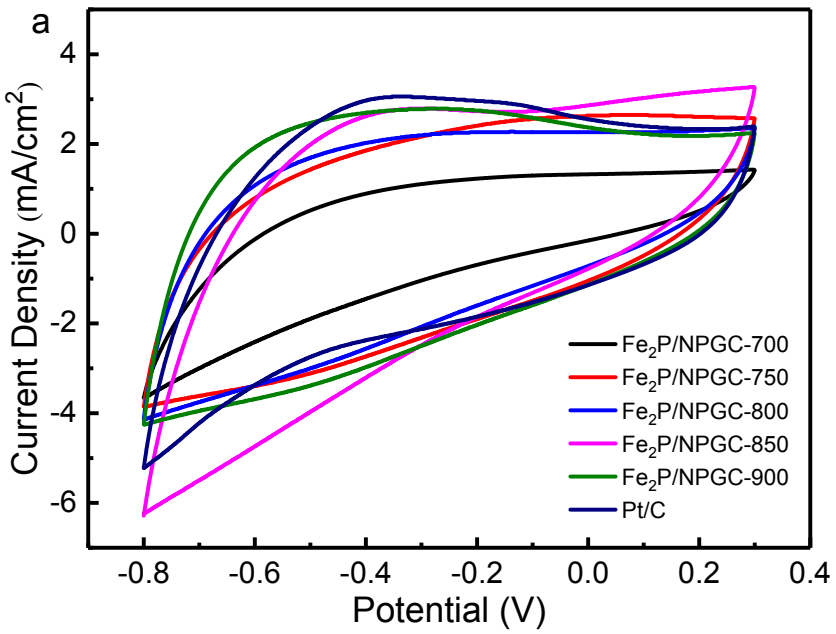

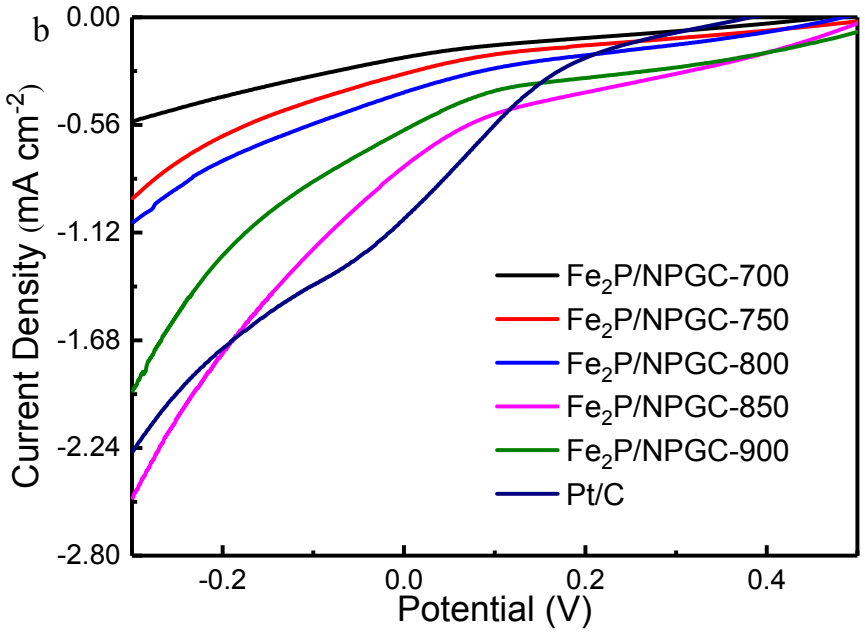

Figure S7. CV (a) and LSV (b) curves of Fe_2P/NPGC-x (x=700, 750, 800, 850 and 900) and Pt/C.

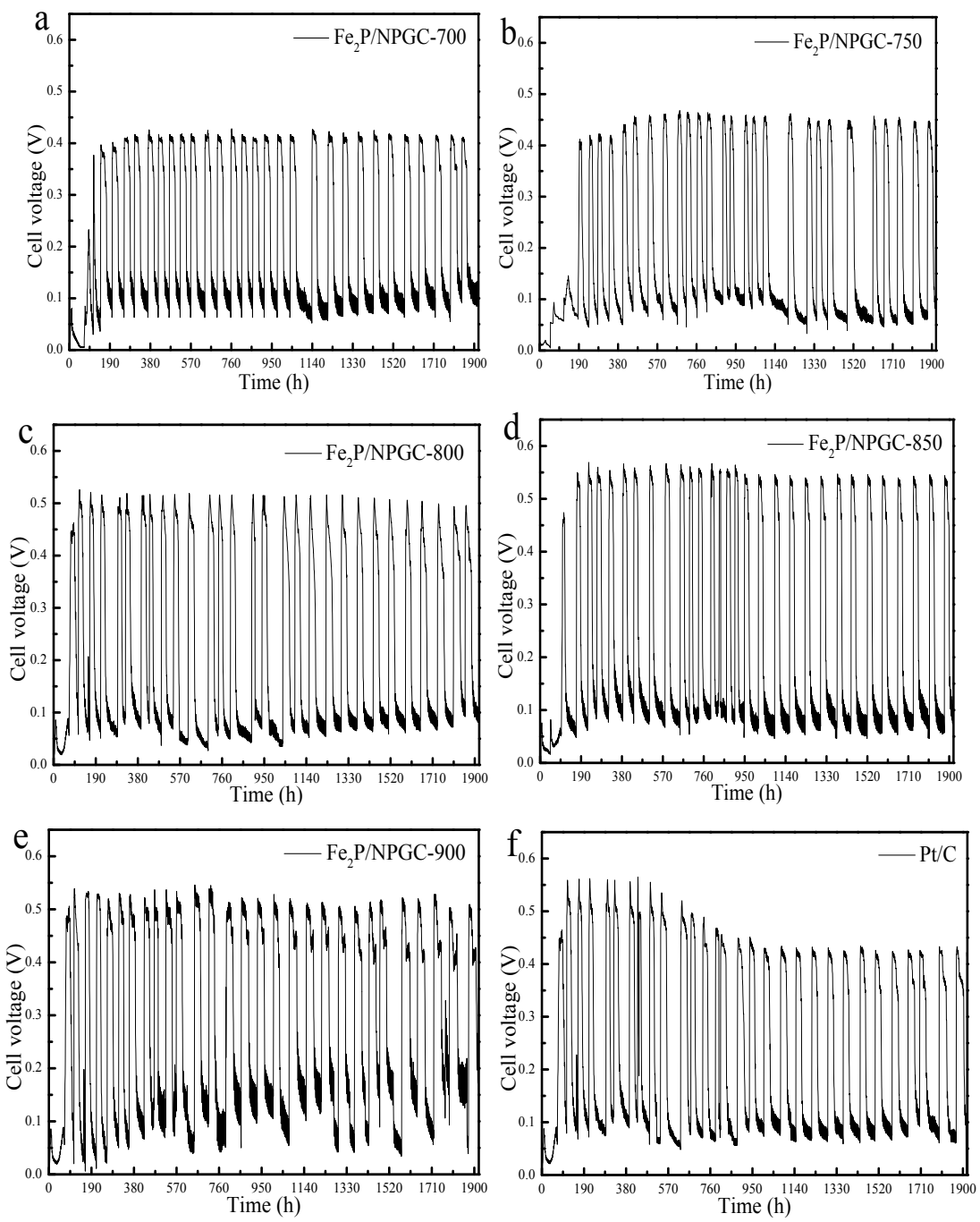

Figure S8. Voltage output of MFCs with the Fe_2P/NPGC-x (x=700 (a), 750 (b), 800 (c), 850 (d), and 900 (e)) and Pt/C (f) cathodes.

References

(1) Jing, B. J.; You, S. J.; Ma, Y. Y.; Xing, Z. P.; Chen, H.; Dai, Y.; Zhang, C. Y.; Ren, N. Q.; Zou, J. L. Fe_3Se_4/FeSe Heterojunctions in Cornstalk-Derived N-Doped Carbon Framework Enhance Charge Transfer and Cathodic Oxygen Reduction Reaction to boost Bio-Electricity Generation. Appl. Catal., B **2019**, *244*, 465-474, DOI 10.1016/j.apcatb.2018.11.074.

(2) Pan, S. Y.; Cai, Z.; Duan, Y. Q.; Yang, L.; Tang, B.; Jing, B. J.; Dai, Y.; Xu, X.; Zou, J. L. Tungsten Diselenide/Porous Carbon with Sufficient Active Edge-Sites as a Co-Catalyst/Pt-Support Favoring Excellent Tolerance to Methanol-Crossover for Oxygen Reduction Reaction in Acidic Medium. Appl. Catal., B **2017**, *219*, 18-29, DOI 10.1016/j.apcatb.2017.07.011.

(3) Hao, L.; Yu, J.; Xu, X.; Yang, L.; Xing, Z. P.; Dai, Y.; Sun, Y.; Zou, J. L. Nitrogen-Doped MoS_2/Carbon as Highly Oxygen-Permeable and Stable Catalysts for Oxygen Reduction Reaction in Microbial Fuel Cells. J. Power Sources **2017**, *339*, 68–79, DOI 10.1016/j.jpowsour.2016.11.041.

(4) Dong, H.; Yu, H. B.; Wang, X.; Zhou, Q. X.; Feng, J. L. A Novel Structure of Scalable Aircathode without Nafion and Pt by Rolling Activated Carbon and PTFE as Catalyst Layer in Microbial Fuel Cells. Water Res. **2012**, *46*, 5777–5787, DOI 10.1016/j.watres.2012.08.005.

(5) Watson, V. J.; Delgado, C. N.; Logan, B. E. Influence of Chemical and Physical Properties of Activated Carbon Powders on Oxygen Reduction and Microbial Fuel Cell Performance. Environ. Sci. Technol. **2013**, *47*, 6704–6710, DOI 10.1021/es401722j.

(6) X. Xu, S.J. You, L. Yang, Z.P. Xing, S.Y. Pan, Z. Cai, Y. Dai, J.L. Zou, Highly Efficient Charge Transfer in Co/Co_2P Schottky Junctions Embedded in Nitrogen-Doped Porous Carbon for Enhancing Bioelectricity Generation, Biosens. Bioelectron. **2018**, *102*, 101-105, DOI 10.1016/j.bios.2017.11.022.

(7) Xiong, C.; Wei, Z. D.; Hu, B. H.; Chen, S. G.; Li, L.; Guo, L.; Ding, W.; Liu, X.; Ji, W. J.; Wang, X. P. Nitrogen-Doped Carbon Nanotubes as Catalysts for Oxygen Reduction Reaction. J. Power Sources **2012**, *215*, 216-220, DOI 10.1016/j.jpowsour.2012.04.057.

(8) Zhao, A. Q.; Masa, J.; Xia, W.; Maljusch, A.; Willinger, M. G.; Clavel, G.; Xie, K.; Schloegl, R.; Schuhmann, W.; Muhlert, M. Spinel Mn-Co Oxide in N-Doped Carbon Nanotubes as a Bifunctional Electrocatalyst Synthesized by Oxidative Cutting. J. Am. Chem. Soc. **2014**, *136*, 7551-7554, DOI 10.1021/ja502532y.

(9) Lv, Y.; Lin, Y. H.; Yang, L.; Cai, Z.; Jing, B. J.; Yu, J.; Jiang, X.; Xing, Z.; Zou, J. L. Iron (III) Metaphosphate/Iron Phosphide Heterojunctions Embedded in Partly-Graphitized Carbon for Enhancing Charge Transfer and Power Generation in Microbial Fuel Cells. Chem. Eng. J. **2018**, *342*, 228-237, DOI 10.1016/j.cej.2018.02.083.

(10) Feng, L. G.; Chang, J. F.; Jiang, K.; Xue, H. G.; Liu, C. P.; Cai, W. B.; Xing, W.; Zhang, J. J. Nanostructured Palladium Catalyst Poisoning Depressed by Cobalt Phosphide in the Electro-oxidation of Formic Acid for Fuel Cells. Nano Energy **2016**, *30*, 355-361, DOI 10.1016/j.nanoen.2016.10.023.

(11) Arrigo, R.; Schuster, M. E.; Xie, Z.; Yi, Y.; Wowsnick, G.; Sun, L. L.; Hermann, K. E.; Friedrich, M.; Kast, P.; Haevecker, M.; Knop-Gericke, A.; Schloegl, R. Nature of the N-Pd Interaction in Nitrogen-Doped Carbon Nanotube Catalysts. ACS Catal. **2015**, *5*, 2740-2753, DOI 10.1021/acscatal.5b00094.

(12) Tian, J. Q.; Liu, Q.; Liang, Y. H.; Xing, Z. C.; Asiri, A. M.; Sun, X. P. FeP Nanoparticles Film Grown on Carbon Cloth: An Ultrahighly Active 3D Hydrogen Evolution Cathode in Both Acidic and Neutral Solutions. ACS Appl. Mater. Interfaces **2014**, *6*, 20579-20584, DOI 10.1021/am5064684.

(13) Yang, W.; Chata, G.; Zhang, Y. D.; Peng, Y.; Lu, J. E.; Wang, N.; Mercado, R.; Li, J.; Chen, S. W. Graphene Oxide-Supported Zinc Cobalt Oxides as Effective Cathode Catalysts for Microbial Fuel Cell: High Catalytic Activity and Inhibition of Biofilm Formation. Nano Energy **2019**, *57*, 811-819, DOI 10.1016/j.nanoen.2018.12.089.

(14) Xu, X.; Dai, Y.; Yu, J.; Hao, L.; Duan, Y. Q.; Sun, Y.; Zhang, Y. H.; Lin, Y. H.; Zou, J. L.

Metallic State FeS Anchored (Fe)/Fe_3O_4/N-Doped Graphitic Carbon with Porous Sponge-Like Structure as Durable Catalysts for Enhancing Bioelectricity Generation. ACS Appl. Mater. Interfaces **2017**, *9*, 10777-10787, DOI 10.1021/acsami.7b01531.

(15) Tian, X. Y.; Zhou, M. H.; Tan, C. L.; Li, M.; Liang, L.; Li, K.; Su, P. KOH Activated N-Doped Novel Carbon Aerogel as Efficient Metal-Free Oxygen Reduction Catalyst for Microbial Fuel Cells. Chem. Eng. J. **2018**, *348*, 775-785, DOI 10.1016/j.cej.2018.05.007.

(16) Shahbazi Farahani, F.; Mecheri, B.; Reza Majidi, M.; Costa de Oliveira, M. A.; D'Epifanio, A.; Zurlo, F.; Placidi, E.; Arciprete, F.; Licoccia, S. MnO_x-Based Electrocatalysts for Enhanced Oxygen Reduction in Microbial Fuel Cell Air Cathodes. J. Power Sources **2018**, *390*, 45-53, DOI 10.1016/j.jpowsour.2018.04.030.

(17) Zhang, L. H.; Hu, Y. Y.; Chen, J. F.; Huang, W. T.; Cheng, J. H.; Chen, Y. C. A novel Metal Organic Framework-Derived Carbon-Based Catalyst for Oxygen Reduction Reaction in a Microbial Fuel Cell. J. Power Sources **2018**, *384*, 98-106, DOI 10.1016/j.jpowsour.2018.02.078.

(18) Hu, Z. X.; Zhou, X. X.; Lu, Y.; Jv, R.; Liu, Y.; Li, N.; Chen, S. W. $CoMn_2O_4$ Doped Reduced Graphene Oxide as an Effective Cathodic Electrocatalyst for ORR in Microbial Fuel Cells. Electrochim. Acta **2019**, *296*, 214-223, DOI 10.1016/j.electacta.2018.11.004.

(19) Papiya, F.; Nandy, A.; Mondal, S.; Kundu, P. P. Co/Al_2O_3-rGO Nanocomposite as Cathode Electrocatalyst for Superior Oxygen Reduction in Microbial Fuel Cell Applications: The Effect of Nanocomposite Composition. Electrochim. Acta **2017**, *254*, 1-13, DOI 10.1016/j.electacta.2017.09.108

(20) Nguyen, M. T.; Mecheri, B.; Iannaci, A.; D'Epifanio, A.; Licoccia, S. Iron/Polyindole-Based Electrocatalysts to Enhance Oxygen Reduction in Microbial Fuel Cells. Electrochim. Acta **2016**, *190*, 388-395, DOI 10.1016/j.electacta.2015.12.105.